The Intrinsic Size of Sagittarius A* from 0.35 cm to 6 cm

Geoffrey C. Bower[1], W.M. Goss[2], Heino Falcke[3], Donald C. Backer[1], Yoram Lithwick[4]

ABSTRACT

We present new high-resolution observations of Sagittarius A* at wavelengths of 17.4 to 23.8 cm with the Very Large Array in A configuration with the Pie Town Very Long Baseline Array antenna. We use the measured sizes to calibrate the interstellar scattering law and find that the major axis size of the scattering law is smaller by $\sim 6\%$ than previous estimates. Using the new scattering law, we are able to determine the intrinsic size of Sgr A* at wavelengths from 0.35 cm to 6 cm using existing results from the VLBA. The new law increases the intrinsic size at 0.7 cm by $\sim 20\%$ and $< 5\%$ at 0.35 cm. The intrinsic size is 13^{+7}_{-3} Schwarzschild radii at 0.35 cm and is proportional to λ^{γ}, where γ is in the range 1.3 to 1.7.

Subject headings: Galaxy: center — galaxies: active — techniques: interferometric — scattering

1. Introduction

Imaging the radio emitting region surrounding the massive black hole in the Galactic Center, Sagittarius A*, has been a goal since its discovery (Balick & Brown 1974). Turbulent electrons along the line of sight to Sgr A*, however, scatter radio wavelength photons and produce an image that is an elliptical Gaussian with a major axis size of ~ 0.5 arcsec at 20 cm and a λ^2 dependence (Backer 1978). Separating the effects of the small intrinsic source from the effects of scattering has required observations at short wavelengths, careful calibration, and the use of closure amplitude techniques, which reduce sensitivity but remove uncertainty

[1]Astronomy Department & Radio Astronomy Laboratory, University of California, Berkeley, CA 94720; gbower,dbacker@astro.berkeley.edu

[2]National Radio Astronomy Observatory, P.O. Box 0, Socorro NM 87801, U.S.A. ; mgoss@nrao.edu

[3]ASTRON, Postbus 2, 7990 AA Dwingeloo, The Netherlands and Department of Astrophysics, Radboud Universiteit Nijmegen, Postbus 9010, 6500 GL Nijmegen, The Netherlands ; falcke@astron.nl

[4]CITA, University of Toronto, 60 St. George Street, Toronto, Ontario, M5S 3H8; yoram@cita.utoronto.ca

due to calibration error (e.g., Bower et al. 2004; Shen et al. 2005). These efforts have recently resulted in the first robust detections of intrinsic structure in Sgr A* at wavelengths of 1.3 cm, 0.7 cm and 0.35 cm. The intrinsic source has a size that scales with $\lambda^{1.1}$ or $\lambda^{1.6}$ to a minimum of ~ 10 Schwarzschild radii at 0.35 cm (assuming $M_{bh} = 4 \times 10^6 M_\odot$ and $d = 8$ kpc ; Ghez et al. (2005); Eisenhauer et al. (2003)).

These detections of the intrinsic size of Sgr A* have a number of consequences. The brightness temperature of 10^{10} K strongly excludes advection dominated accretion flows (ADAFs; Narayan et al. 1998) and Bondi-Hoyle accretion models (Melia 1994). These size measurements, however, cannot differentiate between jet models (Falcke et al. 1993), generic radiatively inefficient accretion flows (Quataert & Gruzinov 2000), and hybrids of these models (Yuan et al. 2002). This limitation is principally due to the limited sensitivity in the minor axis size of the scattering ellipse. Coupled with measurements of the proper motion of Sgr A* (Reid & Brunthaler 2004), the assumption that the black hole is smaller than the emission region implies a lower limit to the mass density of the black hole $\sim 10^5 M_\odot \mathrm{AU}^{-3}$, which strongly excludes alternative models for dark mass objects.

The scattering medium itself is a system of intense interest (Lazio & Cordes 1998; Bower et al. 2001; Goldreich & Sridhar 2006). The λ^2 size dependence of Sgr A* is a strict consequence of the strong scattering and the short projected baselines at the distances of the scattering medium (Narayan & Goodman 1989).

We present here detailed measurements of the scattering properties at wavelengths that range from 17.4 to 23.8 cm using the Very Large Array and the Pie Town Very Long Baseline Array antenna (§2). The addition of the PT antenna to the VLA A configuration improves the East-West resolution by a factor of two. The resulting scattering law is smaller by $\sim 6\%$ than previous estimates. The independent estimate of the scattering law enables us to measure the intrinsic size of Sgr A* at a wavelength as long as 6 cm (§3). We discuss these results in (§4).

We wish to clarify here the numerous axes and steps involved in translating observations of Sgr A* into a measurement of the intrinsic size. VLA observations of Sgr A* are obtained with a synthesized beam that is extended North-South. Deconvolution of the observed image with the synthesized beam gives the apparent, scatter-broadened image of Sgr A*. This image is predominantly a two-dimensional Gaussian with the major axis oriented ~ 80 degrees East of North. Throughout this paper when we refer to the major and minor axes, we refer to the orientation of the scattering Gaussian. Finally, to obtain the intrinsic image, we deconvolve the apparent image with a model of the scatter-broadened image, which is determined from long wavelength apparent sizes.

2. Observations and Analysis

We obtained new observations of Sgr A* with the Very Large Array plus the Pie Town VLBA antenna. The VLA was in the A configuration. Observations were made on 1 and 4 October 2004 in eight separate bands centered at 25.2, 23.8, 23.2, 21.9, 20.9, 19.8, 18.0, and 17.5 cm. Each band had 12.5 MHz bandwidth with 15 channels. Results at 25.2 and 21.9 cm were corrupted by interference and we do not consider these data any further.

We calibrated the absolute flux density with observations of 3C 286. Corrections for atmospheric and instrumental amplitude and phase fluctuations were made through self-calibration of frequent observations of the compact source J1744-312. We imaged Sgr A* using baselines longer than $50k\lambda$ and uniform weighting to suppress large-scale structure (Figure 1).

The presence of a radio transient with a flux density of $\sim$ 30 mJy and a resolved morphology at a separation of $2.7''$ South of Sgr A* precluded modeling in the visibility and closure amplitude domains (Bower et al. 2005). We previously showed that fitting in the image domain provides results that are equivalent to fitting in the closure amplitude domain at centimeter wavelengths, in the case where the difficulty of calibration and poor telescope performance are less critical (Bower et al. 2001, 2004). Long wavelength data obtained from the VLA meet these criteria better than any other data. Accordingly, we fit sizes to Sgr A* in the image plane with a region that excluded most of the transient flux density. The effect of the transient is primarily on the accuracy of the size in the minor axis of the scattering angle. The synthesized beam ranges from 1.69×0.56 arcsec at 17.5 cm to 2.36×0.98 arcsec at 23.8 cm, oriented roughly North-South. Measured sizes ranged from 1.71×0.67 arcsec at 17.5 cm and 2.43×1.22 arcsec at 23.8 cm. Sgr A* is clearly resolved in both axes but with considerably more accuracy in the East-West axis than an in the North-South axis. Fitting a point source to the data produced very poor quality fits, while fitting an elliptical Gaussian produced a residual image with no obvious systematic errors and an rms $\sim$ 2.5 mJy/beam (Figure 1). This rms is a few times the rms $\sim$ 0.9 mJy/beam determined far away from Sgr A*, possibly due to the presence of confusing emission around Sgr A*.

We deconvolved the measured Gaussian sizes with the synthesized beam sizes to determine the true source parameters: total flux density, major axis, minor axis, and position angle. We determined errors in the parameters by calculating χ^2 for a grid in the parameters surrounding the best-fit value. These errors are the formal uncertainy in the parameters and do not reflect the systematic errors, which we discuss below. Results are tabulated in Table 1.

In the case of the minor axis, there is a clear trend of decreasing size with decreasing

wavelength, which indicates the presence of systematic errors. Marginal resolution of Sgr A* in the North-South axis and confusion from the presence of the radio transient due South of Sgr A* are the likely causes of this effect. The major axis size, however, is not affected by the transient and only weakly distorted by changes in the position angle; the best-fit solution for major axis size changes by only 1% with a 10° change in position angle. We conclude that the results determined from the VLA+PT result are accurate in the major axis but not in the minor axis.

We experimented with a range of imaging parameters to explore systematic effects on the deconvolved size of Sgr A*. Weighting with a robustness parameter of 0, using super-uniform weighting, and changing the minimum (u, v) distance from 40 to 100 $k\lambda$ changed the deconvolved major axis size by no more than 3%. Since the results are strongly dependent on the PT antenna, we dropped random groups of 5 baselines associated with PT, producing 1% changes in the deconvolved size. These errors are comparable to those found for other sources through VLA observations (e.g., Trotter et al. 1998). Thus, our results are influenced by systematic imaging effects at a level of a factor of no more than a few. As we discuss below, a factor of a few is consistent with the scatter in the measurements.

3. The Scattering Size and The Intrinsic Size of Sgr A*

In Figure 2, we plot the measured size of Sgr A* from the VLA+PT observations and from Very Long Baseline Array results from Bower et al. (2004) at wavelengths of 6.01 cm to 0.67 cm. We also include the VLBA result from Shen et al. (2005) at 0.35 cm. The sizes are plotted normalized by wavelength squared.

We fit a power law of the form λ^2 to the major axis sizes using the new VLA+PT results at 17.4 to 23.8 cm wavelength. The best-fit value to the normalization of the scattering law is 1.309 ± 0.017 mas/cm^2. The errors in these values are determined from the scatter in the measurements. The best-fit scattering values are plotted as a straight line in Figure 2. The major axis normalization is $\sim 6\%$ smaller than previous estimates. None of our measurements are consistent with the previously determined major axis normalization of 1.39 mas/cm^2. The best estimates of the minor axis scattering size and position angle remain the results determined previously from VLBA observations at wavelengths between 2 cm and 6 cm ($0.64^{+0.04}_{-0.05}$ mas/cm^2 and $78^{+0.8}_{-1.0}$ deg; Bower et al. 2004).

The scatter in the VLA+PT major axis sizes is much larger than the expectation of the statistical errors for individual points. The reduced $\chi^2_\nu \approx 7$ for the major axis, indicating that there are additional sources of error in the measurement of the size that we are not including.

Dropping either the two highest frequency or two lowest frequency VLA+PT sizes did not significantly affect the reduced χ^2 or the best-fit scattering law. We also explored the effect of the inclusion of the shorter wavelength VLBA results on the major axis scattering size. Inclusion of the 6 cm size decreases the reduced χ^2_ν slightly but does not affect the scattering size significantly. Inclusion of VLBA results at wavelengths of 3.6 cm and shorter, however, leads to a significant increase in χ^2_ν to 18. That is, the major axis sizes at $\lambda <= 3.6$ cm are not consistent with the longer wavelength sizes and a λ^2 scattering law. This inconsistency holds if we scale the VLA+PT errors by a factor as large as 5, which reveals $\chi^2_\nu = 1.8$.

The λ^2 dependence of the scattering law is strongly favored for theoretical reasons. The maximum baseline length projected to the scattering region is $b_{proj} = D_{scattering}/D_{SgrA} \times b_{max} \sim 1km$, where $D_{SgrA} = 8$ kpc is the distance to Sgr A*, $D_{scattering} \approx 100$ pc is the distance of the scattering region from Sgr A*, and $b_{max} \approx 70$ km is the maximum baseline between the VLA and PT. b_{proj} is substantially smaller than the expected and measured inner scales (b_{inner}) for the power spectrum of turbulent fluctuations (10^2 to $10^{5.5}$ km; Wilkinson et al. (1994)). This result holds for the long VLBA baselines involved in imaging at shorter wavelengths, as well, where $b_{proj} \sim 25$ km at 0.7 cm wavelength. For the case of $b_{proj} << b_{inner}$, the resulting image is very heavily averaged and must be Gaussian in shape with size $\propto \lambda^2$ (Narayan & Goodman 1989).

This expectation of strong scattering is supported by previous measurements of the shape of the image of Sgr A*. Bower et al. (2004) showed that fitting the closure amplitudes of Sgr A* at 0.7 cm with a functional form for the visibilities of $\propto e^{-b^{(\beta-2)}}$, where b is the baseline length, revealed $\beta = 4.00 \pm 0.03$. That is, the best evidence indicates that the image of Sgr A* is a Gaussian. Following scattering theory, where the size is proportional to λ^α, then $\alpha = \beta - 2 = 2.00 \pm 0.03$ (Narayan & Goodman 1989). For the case of the VLA+PT data, we find $\alpha = 1.98 \pm 0.11$, which is consistent with the expectation of $\alpha = 2$.

Nevertheless, if we fit a single power-law to all of the VLA+PT and VLBA data, we find $\alpha = 1.96 \pm 0.01$ with a $\chi^2_\nu = 5.5$. So, without the constraint of a λ^2 size for the scattering law at some wavelength, the evidence for resolving an intrinsic size becomes marginal at any wavelength. A fit of the size proportional to $\sqrt{a^2\lambda^4 + b^2\lambda^{2\gamma}}$ produces an apparent size very similar to that of the single index power-law fit but is not sufficiently constrained to set reasonable limits on the parameters. If we fix γ and search for a and b, we find that χ^2 for $\gamma = 1$ is four times the value for γ unconstrained, indicating that $\gamma = 1$ is strongly excluded. Without the assumption that the second term is negligible for wavelengths longer than 6 cm, therefore, we cannot determine the scattering law or the intrinsic size of Sgr A*.

A final caveat is required. The scattering medium is dynamic. The minimum time scale for a change in the medium is the refractive time scale, which is $0.5y(v/100km/s)(\lambda/1cm)^2$

for Sgr A*, where v is the velocity of the scattering material relative to Sgr A* and the Sun (Narayan & Goodman 1989). The data presented here were obtained in a span of roughly a decade. The long-wavelength scattering properties are very unlikely to change on this time scale. However, at wavelengths as long as 4 cm, the refractive time scale is < 10 year. The many observations at 0.7 cm in this period, however, appear to produce a source of stable size, despite a refractive time scale less than one year. We conclude it is unlikely that the scattering size has changed significantly over this period.

With the assumption that the scattering law is determined accurately at wavelengths longer than 17 cm, we can determine the intrinsic size. We subtract in quadrature the scattering law size from the measured size (Table 2, Figure 3). We compute the results for the best-fit major axis scattering law ($b_{sc} = 1.31$ mas/cm^2), and $\pm 3\sigma$ of the best-fit value. For the best-fit case, the intrinsic size is accurately determined from 0.35 cm to 3.6 cm. Over this range, the intrinsic size is well-fit by a power-law λ^{γ}, where $\gamma = 1.6 \pm 0.1$. For the smaller scattering size, we find a steeper power-law and measure the intrinsic size from 0.35 cm to 6 cm. For the larger scattering size, we cannot measure the intrinsic size at wavelengths longer than 1.3 cm and find a shallower power-law index of $\gamma = 1.3 \pm 0.2$.

If the intrinsic size power-law extends to $\lambda \sim 20$ cm, the contribution of the intrinsic size results in an increase of the measured angular sizes by $\sim 1.5\%$. This is comparable to the error in the major axis scattering law and, therefore, negligible.

4. Discussion

We have measured the intrinsic size of Sgr A* from 0.35 to 3.6 cm. At short wavelengths, the result is consistent with the conclusions of recent efforts by Bower et al. (2004) and Shen et al. (2005). The size of Sgr A* at 0.35 cm is $13.3^{+6.7}_{-3.1} R_s$, where $R_s = 1.2 \times 10^{12}$ cm is the Schwarzschild radius for $M_{bh} = 4 \times 10^6 M_{\odot}$ and the Galactic Center distance $d = 8$ kpc. This compact size confirms tight restrictions on accretion models and black hole alternatives previously claimed and stated in §1.

The wavelength dependence of the source size agrees with that found by Bower et al. (2004) and is steeper than that found by Shen et al. (2005), who found $\gamma \approx 1.1$. The steeper dependence indicates that the brightness temperature decreases as λ^{-1}, assuming that the size in the second dimension is proportional to the major axis size. The peak brightness temperature at 0.35 cm is $\sim 10^{10}$ K for a flux density of 1 Jy. The power-law dependence of the size as a function of wavelength indicates a stratified, smoothly varying emission region.

Detailed jet models for Sgr A* predict $\gamma \approx 1$ (Falcke & Markoff 2000). Generalized

jet models, however, allow a range of γ, depending on the details of the magnetic field and particle energy density distributions (e.g., Konigl 1981). A jet with $B \propto r^{-1}$, electron density decreasing as r^{-1}, and optically thin power-law index of 1 will show a size $\propto \lambda^{1.4}$.

Yuan et al. (2006) model the size of Sgr A* for a radiatively inefficient accretion flow. They fit sizes at 0.35 cm and 0.7 cm that are fit with a power law of index $\gamma = 1.1$. Variations in the nonthermal electron distribution or deviations from equipartition, however, could alter γ in their model.

The critical remaining observational goals for understanding the image of the radio emission of Sgr A* are a measurement of the two-dimensional size and detection of structural variability. The simple one-dimensional deconvolution that we have performed here only gives schematic information on the size of Sgr A*. With a more accurate two-dimensional scattering model, future analysis will directly compare the observed image with non-Gaussian source models convolved with the imaging and scattering constraints. Astrometric observations may indicate a shift in the centroid of the image with frequency. A heterogeneous jet will exhibit such a shift due to changing location of the optically thick surface of the source (Konigl 1981).

At mm and submm wavelengths, the gravity of the black hole will distort the image (Falcke et al. 2000; Broderick & Loeb 2005). Detailed knowledge of the shape of the longer wavelength image will permit a more accurate characterization of light-bending effects in the actual image. Ultimately, these images will provide one of the strongest tests of the existence and characterization of black holes.

The National Radio Astronomy Observatory is a facility of the National Science Foundation operated under cooperative agreement by Associated Universities, Inc.

REFERENCES

Backer, D. C. 1978, ApJ, 222, L9

Balick, B. & Brown, R. L. 1974, ApJ, 194, 265

Bower, G. C., Backer, D. C., & Sramek, R. A. 2001, ApJ, 558, 127

Bower, G. C., Falcke, H., Herrnstein, R. M., Zhao, J., Goss, W. M., & Backer, D. C. 2004, Science, 304, 704

Bower, G. C., Roberts, D. A., Yusef-Zadeh, F., Backer, D. C., Cotton, W. D., Goss, W. M., Lang, C. C., & Lithwick, Y. 2005, ApJ, 633, 218

Broderick, A. E. & Loeb, A. 2005, MNRAS, 363, 353

Eisenhauer, F., Schödel, R., Genzel, R., Ott, T., Tecza, M., Abuter, R., Eckart, A., & Alexander, T. 2003, ApJ, 597, L121

Falcke, H., Mannheim, K., & Biermann, P. L. 1993, A&A, 278, L1

Falcke, H. & Markoff, S. 2000, A&A, 362, 113

Falcke, H., Melia, F., & Agol, E. 2000, ApJ, 528, L13

Ghez, A. M., Salim, S., Hornstein, S. D., Tanner, A., Lu, J. R., Morris, M., Becklin, E. E., & Duchêne, G. 2005, ApJ, 620, 744

Goldreich, P. & Sridhar, S. 2006, ApJ, 640, L159

Konigl, A. 1981, ApJ, 243, 700

Lazio, T. J. W. & Cordes, J. M. 1998, ApJ, 505, 715

Melia, F. 1994, ApJ, 426, 577

Narayan, R. & Goodman, J. 1989, MNRAS, 238, 963

Narayan, R., Mahadevan, R., Grindlay, J. E., Popham, R. G., & Gammie, C. 1998, ApJ, 492, 554

Quataert, E. & Gruzinov, A. 2000, ApJ, 539, 809

Reid, M. J. & Brunthaler, A. 2004, ApJ, 616, 872

Shen, Z.-Q., Lo, K. Y., Liang, M.-C., Ho, P. T. P., & Zhao, J.-H. 2005, Nature, 438, 62

Trotter, A. S., Moran, J. M., & Rodriguez, L. F. 1998, ApJ, 493, 666

Wilkinson, P. N., Narayan, R., & Spencer, R. E. 1994, MNRAS, 269, 67

Yuan, F., Markoff, S., & Falcke, H. 2002, A&A, 383, 854

Yuan, F., Shen, Z.-Q., & Huang, L. 2006, ApJ, 642, L45

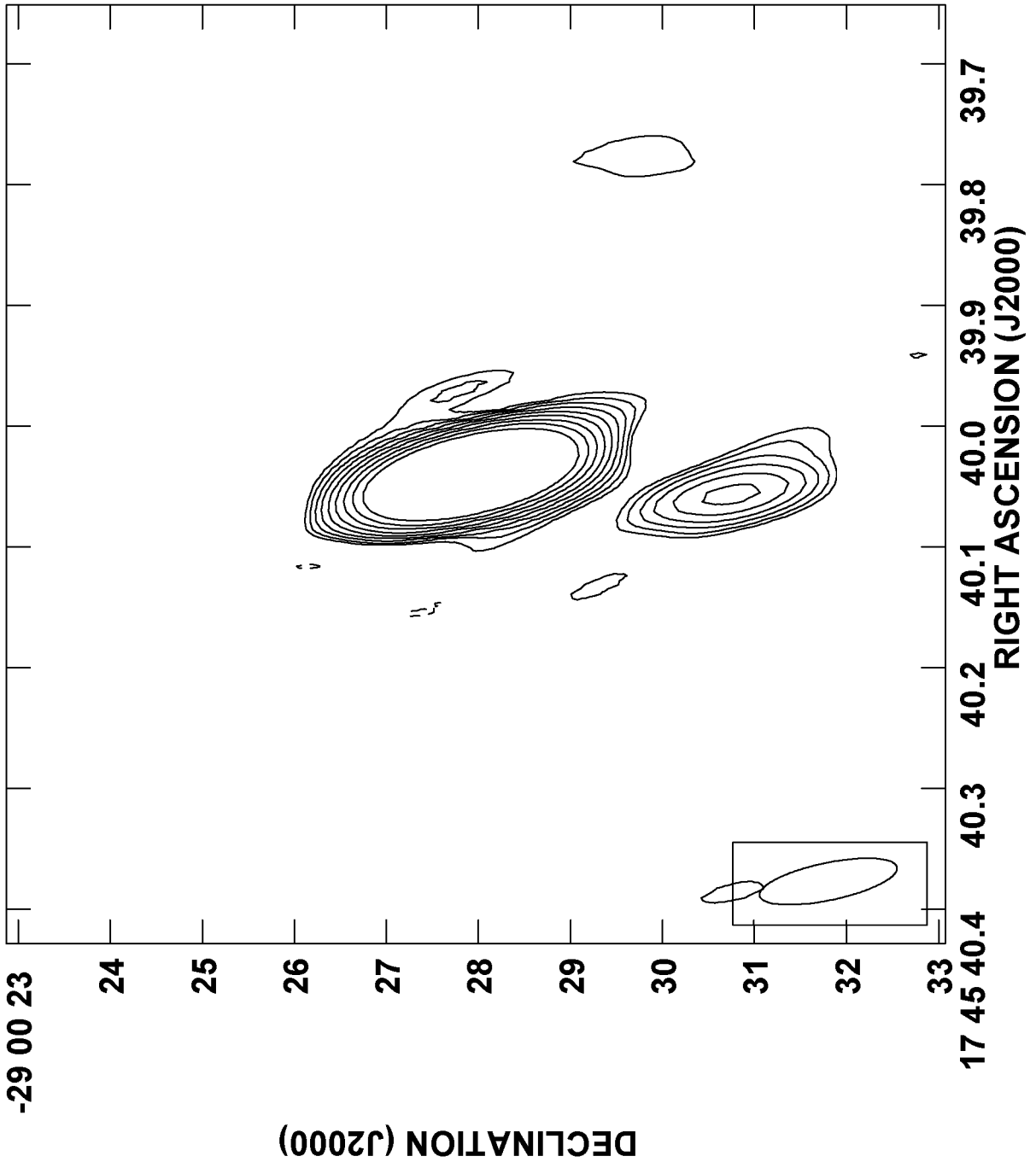

This preprint was prepared with the AAS LaTeX macros v5.2.

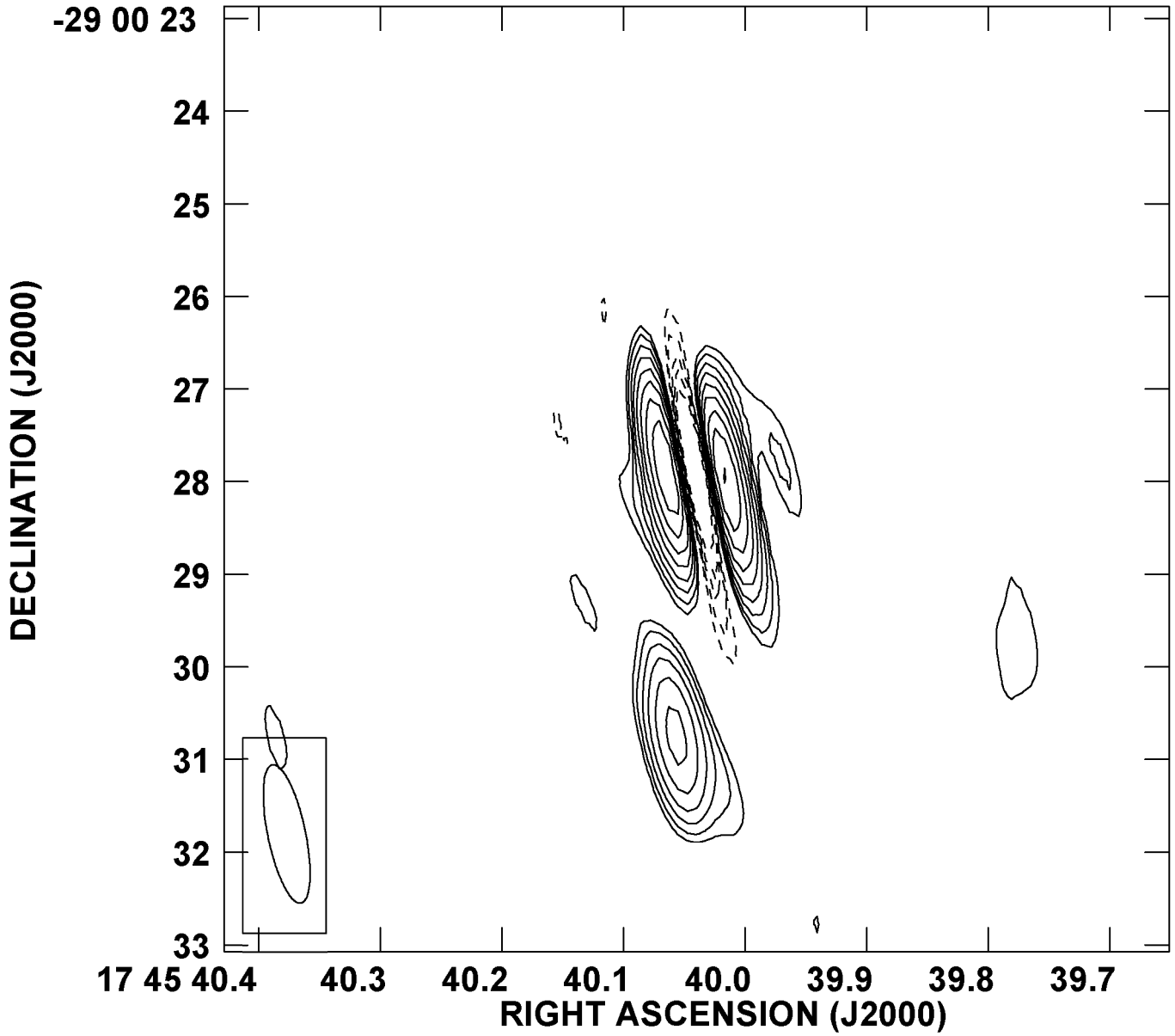
-29 00 23
24
25
26
27
28
29
30
31
32
33
DECLINATION (J2000)
17 45 40.4
40.3
40.2
40.1
40.0
39.9
39.8
39.7
RIGHT ASCENSION (J2000)

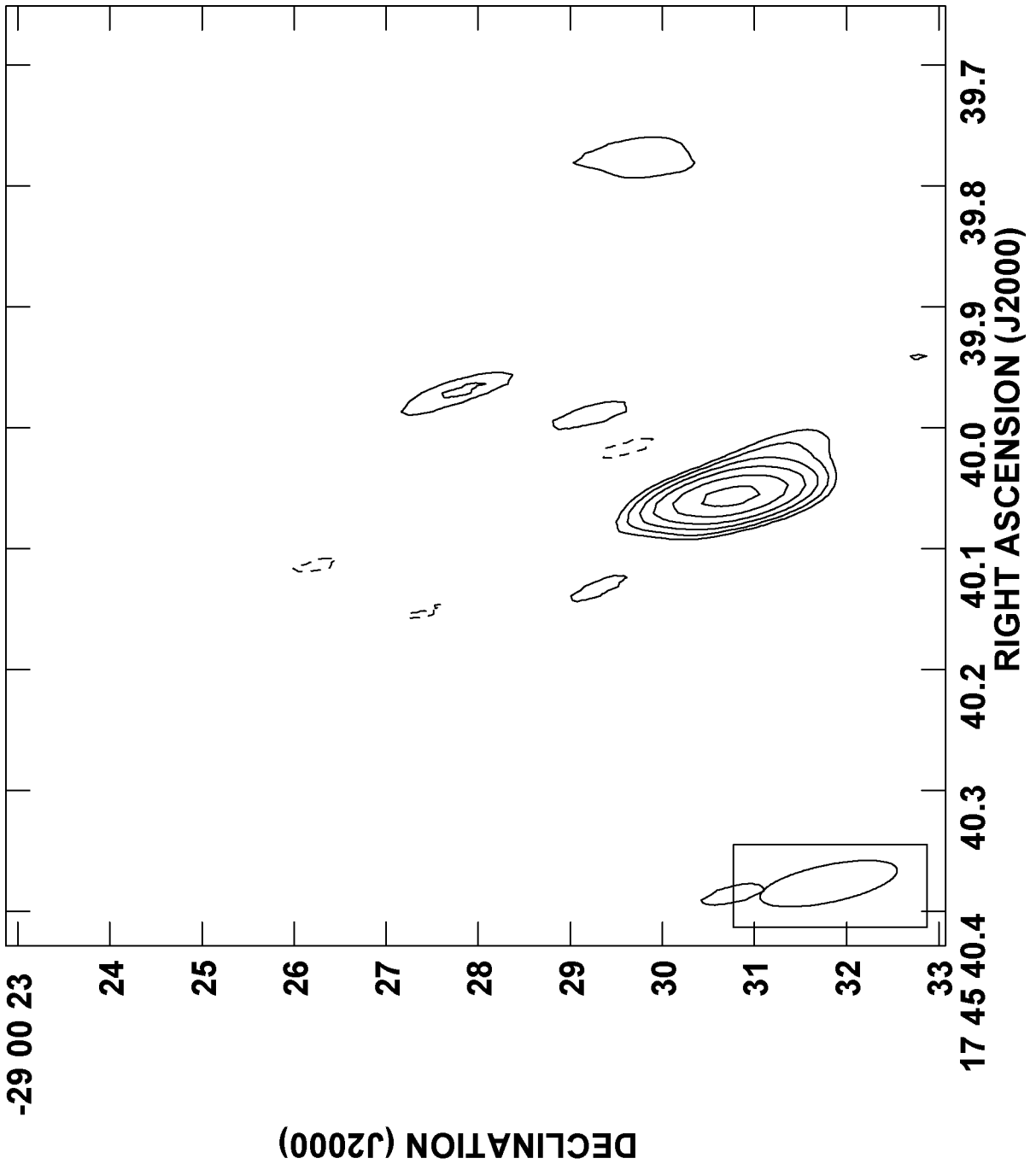

Fig. 1.— (*left*) Image of Sgr A* at 17.5 cm from the VLA+PT observations. Sgr A* is the bright source at the center of the image. The source to the South of Sgr A* is the transient. The synthesized beam size is indicated in the lower part of the image. Contours

begin at 5 mJy/beam and increase by factor of $\sqrt{(2)}$ to half the peak intensity of Sgr A*. The synthesized beam size is 1.69×0.56 arcsec. (*center*) Residual image of Sgr A* after subtraction of best-fit point source. This shows that the source is clearly resolved East-West and at best marginally resolved North-South. (*right*) Residual image of Sgr A* after subtraction of best-fit Gaussian source. The source is well-modeled to an rms of 2.5 mJy/beam.

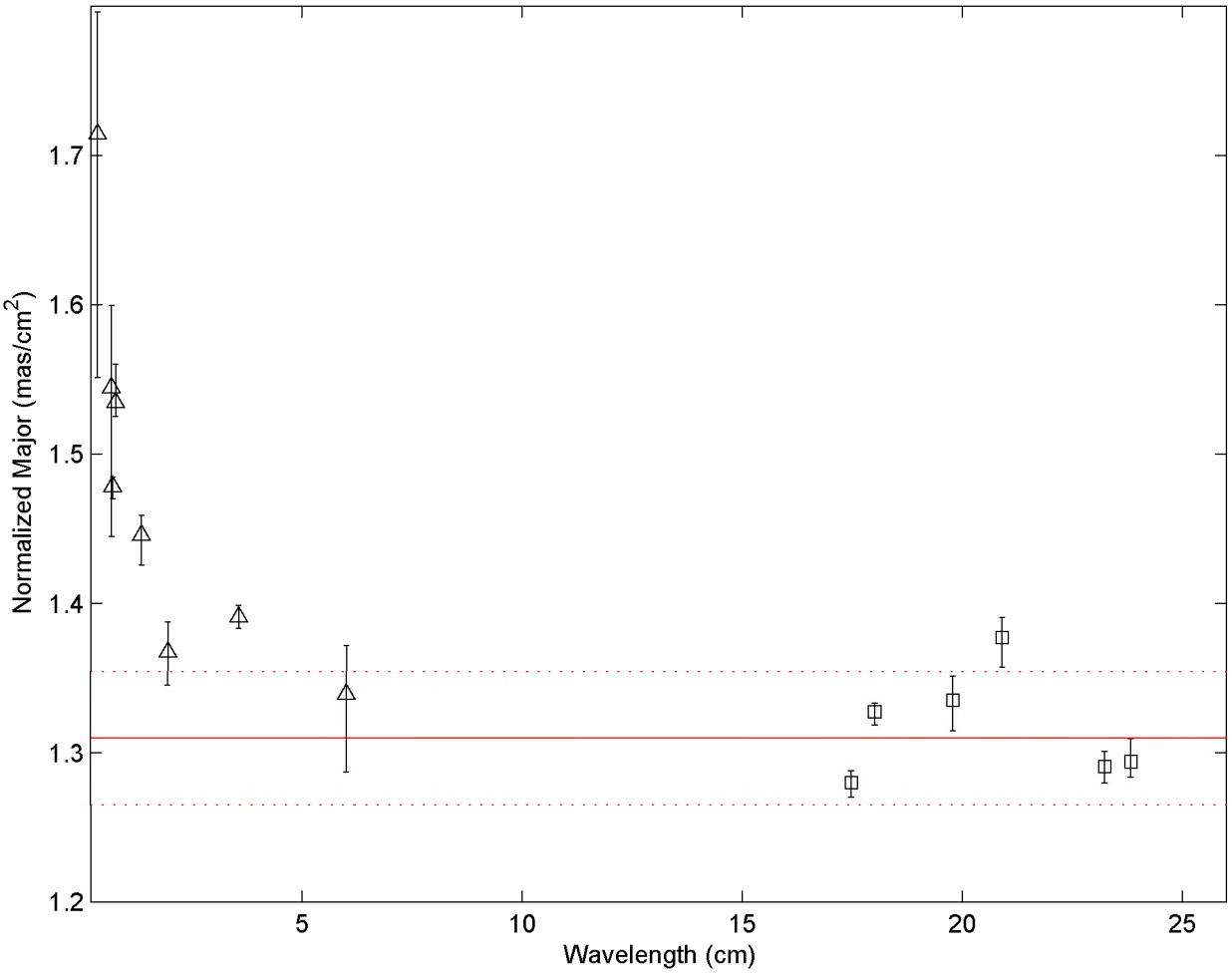

Fig. 2.— Measured major axis size as a function of wavelength. Triangles are VLBA measurements determined through closure amplitude analysis from Bower et al. (2004) and Shen et al. (2005). Squares are the new VLA+PT measurements. The major axis sizes have been normalized by λ^2. The solid red line is the best-fit scattering value determined from the VLA+PT data alone. Dotted red lines are $\pm 3\sigma$ of the best-fit scattering law.

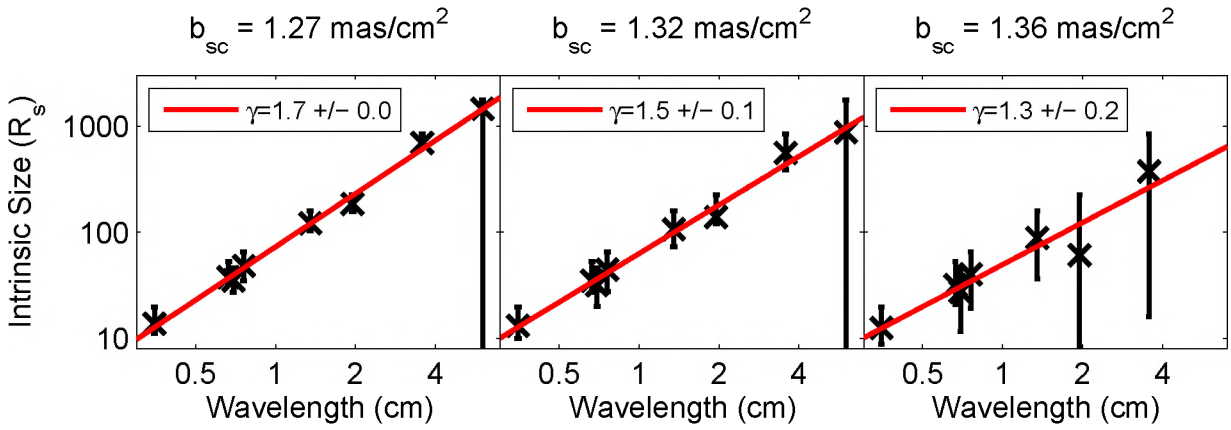

Fig. 3.— Intrinsic size in Schwarzschild radii for the East-West dimension using three different estimates of the major axis scattering law. We assume a $4 \times 10^6 M_\odot$ black hole at a distance of 8 kpc. In the central panel, we show results for the best-fit scattering law. In the left and right panels, we show the results for the -3σ and $+3\sigma$, respectively. The solid red lines are the best fit curves for size $\propto \lambda^\gamma$.

Table 1. Apparent and Deconvolved Sizes of Sagittarius A* from VLA+PT Observations of October 2004

		Apparent Size			Deconvolved Size			
λ (cm)	Synth. Beam (mas × mas,deg)	b_{maj} (mas)	b_{min} (mas)	PA (deg)	b_{maj} (mas)	b_{min} (mas)	PA (deg)	S (mJy)
23.8	2357×979, 0.1	$2433.5^{+8.2}_{-8.2}$	$1222.6^{+5.2}_{-3.1}$	$-0.21^{+0.14}_{-0.14}$	$734.7^{+8.7}_{-5.9}$	$602.4^{+36.0}_{-29.9}$	$97.7^{+1.1}_{-7.5}$	$471.9^{+1.6}_{-1.6}$
23.2	2191×714, 4.8	$2252.1^{+8.4}_{-5.1}$	$985.5^{+3.0}_{-3.7}$	$5.83^{+0.10}_{-0.10}$	$697.1^{+5.4}_{-5.9}$	$496.3^{+40.1}_{-19.6}$	$76.5^{+2.7}_{-2.1}$	$490.6^{+1.5}_{-1.9}$
20.9	1996×646, 7.6	$2049.4^{+6.1}_{-6.1}$	$849.2^{+2.5}_{-2.5}$	$9.06^{+0.07}_{-0.07}$	$601.8^{+6.0}_{-8.6}$	$397.3^{+27.2}_{-19.1}$	$66.1^{+3.9}_{-2.9}$	$432.1^{+1.3}_{-1.3}$
19.8	1840×581, 10.4	$1877.8^{+5.4}_{-5.4}$	$751.1^{+2.2}_{-2.2}$	$11.92^{+0.06}_{-0.06}$	$522.8^{+6.3}_{-8.0}$	$306.6^{+31.2}_{-21.1}$	$70.5^{+3.7}_{-2.7}$	$441.5^{+1.3}_{-1.3}$
18.0	1737×564, 7.2	$1758.6^{+2.5}_{-2.5}$	$695.9^{+1.0}_{-1.0}$	$8.23^{+0.06}_{-0.06}$	$430.8^{+1.9}_{-2.8}$	$236.7^{+18.6}_{-14.4}$	$74.9^{+1.8}_{-1.3}$	$505.0^{+0.7}_{-0.7}$
17.5	1689×556, 6.8	$1706.4^{+2.5}_{-2.5}$	$667.6^{+1.0}_{-1.0}$	$7.71^{+0.06}_{-0.06}$	$391.2^{+2.4}_{-3.0}$	$206.3^{+21.6}_{-15.5}$	$74.5^{+2.1}_{-1.5}$	$511.9^{+0.7}_{-0.7}$

Note. — The quoted errors in the peak flux density S do not include the $\sim 10\%$ error in absolute flux density.

Table 2. Intrinsic Size of Sagittarius A*

	$b_{sc} = 1.26$ mas/cm^2	$b_{sc} = 1.31$ mas/cm^2	$b_{sc} = 1.36$ mas/cm^2
λ (cm)	Size (mas)	Size (mas)	Size (mas)
0.35	$0.142^{+0.062}_{-0.025}$	$0.136^{+0.069}_{-0.032}$	$0.128^{+0.076}_{-0.040}$
0.67	$0.395^{+0.157}_{-0.047}$	$0.362^{+0.190}_{-0.080}$	$0.324^{+0.228}_{-0.118}$
0.69	$0.373^{+0.110}_{-0.077}$	$0.331^{+0.152}_{-0.120}$	$0.280^{+0.203}_{-0.170}$
0.76	$0.505^{+0.177}_{-0.128}$	$0.461^{+0.221}_{-0.172}$	$0.410^{+0.272}_{-0.223}$
1.35	$1.295^{+0.369}_{-0.174}$	$1.117^{+0.547}_{-0.351}$	$0.897^{+0.767}_{-0.571}$
1.95	$2.028^{+0.408}_{-0.304}$	$1.500^{+0.936}_{-0.223}$	$0.563^{+1.873}_{-0.562}$
3.56	$7.491^{+1.524}_{-0.281}$	$5.953^{+3.062}_{-1.819}$	$3.735^{+5.280}_{-3.732}$
6.01	$16.427^{+2.981}_{-16.410}$	$10.094^{+9.314}_{-10.083}$	$0.000^{+19.408}_{-0.000}$

Note. — The intrinsic size is computed for the best-fit value to the major axis scattering size ($b_{sc} = 1.31$ mas/cm^2) and for $\pm 3\sigma$ values.